Proceedings of ASME Turbo Expo 2018: Turbomachinery Technical Conference and Exposition
GT2018
June 11-15, 2018, Oslo, Norway

GT2018-77129

THE DEVELOPMENT AND TESTING OF A DUAL-ENTRY TURBINE EXPANDER FOR ORC APPLICATIONS

Jeff Noall
Barber Nichols Inc.
Arvada, Colorado, USA
jnoall@barber-nichols.com

Timothy Ernst
Cummins Inc.
Columbus, Indiana, USA
timothy.ernst@cummins.com

ABSTRACT

Reducing the fuel consumption and greenhouse gas emissions of large commercial vehicles is a growing priority as governments around the globe introduce more stringent emissions regulations and as companies work to reduce their carbon footprint. Organic Rankine Cycles (ORC) can be applied to these vehicles to recover power from engine waste heat, thereby increasing efficiency and reducing fuel burn. However, the available waste heat consists of both high and low temperature sources making an efficient and cost-effective utilization of these resources challenging. In order to utilize both waste heat streams effectively, a single rotor, dual-entry turbine expander capable of accepting process flow simultaneously from high and low pressure supplies was developed, manufactured and tested. Test results show that the turbine concept was able to meet performance targets while decreasing the size, cost and complexity of the dual pressure ORC.

NOMENCLATURE

C_o	Isentropic spouting velocity = $\sqrt{2\Delta h_{s,ts}}$.
$\bar{C}_o$	Net isentropic spouting velocity of the LP & HP streams.
$\Delta h_{s,ts}$	$h_{o1} - h_{s2}$
D_{pitch}	Turbine blade pitch (meanline) diameter.
η_{ts}	Turbine adiabatic, isentropic efficiency between inlet total and exit static thermodynamic states.
$\bar{\eta}_{ts}$	Net turbine efficiency of the LP & HP streams.
h_{o1}	Turbine inlet total enthalpy.
h_{o2}	Turbine discharge total enthalpy.
h_{s2}	Turbine discharge adiabatic, isentropic static enthalpy.
$\dot{m}$	Mass flow of the turbine drive gas.
$\dot{m}_{tot}$	Combined turbine mass flow of the high and low pressure streams.
N	Shaft speed.
N_s	Specific speed = $N\sqrt{Q}/(\Delta h_{s,ts})^{0.75}$.
P	Power delivered to the gearbox shaft by the turbine wheel.
PR_{ts}	Turbine inlet total to discharge static pressure ratio.
Q	Turbine discharge volumetric flow rate.
U	Turbine blade pitch line (meanline) wheel speed.
U/C_o	Turbine velocity ratio = blade tangential speed divided by the isentropic spouting velocity.
$\bar{\tau}_c$	Net torque coefficient.
τ	Total torque delivered by the turbine.

Subscripts

LP	Applied to the low pressure fluid stream.
HP	Applied to the high pressure fluid stream.

INTRODUCTION

Reducing fuel usage of Class 8 trucks is a key initiative across the globe as greenhouse gas legislation is enacted and customers demand increased fuel economy. Significant gains in fuel economy from the engine itself are becoming more challenging as advances in engine technology have increased the brake thermal efficiency to the point where it is approaching the theoretical Carnot limit. The application of an Organic Rankine Cycle

(ORC) Waste Heat Recovery (WHR) system to a mobile truck application, such as a Class 8 truck, can provide significant fuel economy gains, however it is challenging due to the packaging, complexity and cost of the system.

Basic ORC systems use a single heat input loop that supplies high pressure, superheated vapor from the heat input source(s) to an expander. The high pressure side of the system is optimized for the temperature of the waste heat stream being utilized. This is accomplished through expander sizing to match the expander flow rate along with the corresponding high side pressure ratio for the given amount of waste heat available. Higher temperature waste heat sources allow the high side pressure, and therefore saturation temperature, to be elevated. This higher pressure allows increased expansion work to be extracted from the working fluid.

The waste heat sources from an engine are at varied temperatures. There is a high fraction of waste heat that is available from the engine coolant at a relatively low temperature compared to the high temperature heat sources of tailpipe exhaust and exhaust gas recirculation (EGR). In order to utilize the low temperature waste heat in a typical ORC cycle, the high side pressure of the ORC must be reduced to enable phase change to occur at the low temperature while extracting this heat. However, reducing the high side pressure to enable lower temperature waste heat to be used also reduces the amount of useful work that can be extracted from the high temperature heat sources. The basic ORC cycle is thus limited in its ability to efficiency produce power from multiple heat sources at varied temperatures.

Several cycle architectures have been studied in an effort to identify configurations that make more efficient and effective use of the available thermal resources. Lecompte et al. [1] investigated the performance improvement potential of a number of alternative ORC configurations. Of these, two architectures, the dual loop and dual pressure cycles, show a significant improvement potential for applications with multiple heat sources, though at the expense of added system complexity and cost [1–9].

Dual loop cycles, also referred to as cascade or two-stage cycles, are essentially two separate ORC loops, each with different pressure and temperature levels. The separate nature of the loops allows for the selection of a different working fluid in each leg based on a determination of the phase change and heat transfer characteristics of available fluids that are best matched to each individual heat source [1, 7]. The main drawbacks of this architecture are the added cost, footprint and complexity associated with having two fluid inventory systems, two sets of pumps and expanders, as well as the requirement for additional, and often more complex, heat exchangers.

Dual pressure cycles are similar to dual loop cycles in their ability to make more efficient use of multiple heat sources, except that dual pressure cycles use the same working fluid in both the high and low pressure loops of the cycle. Although this results in a simpler solution with lower hardware costs, some losses in cycle efficiency may result due to higher heat transfer irreversibilities associated with the use of a working fluid that is not as well matched to one or both of the heat source temperatures. However, for cases where the individual heat source temperatures do not cover a wide range, these added losses may be relatively small, making the dual pressure loop a potentially attractive option [7].

The use of a dual pressure ORC system allows the high side pressure of each individual loop to be optimized for the temperatures of the available waste heat sources. This allows increased gains to be achieved from the high temperature waste heat while still utilizing the low temperature waste heat, thereby resulting in both a higher cycle efficiency and power output. The added cost associated with the duplicated hardware of this configuration (pumps, expanders, heat exchangers, etc.) can be a significant hurdle for making the economic case to implement the cycle [8].

The expander is often one of the highest single item costs for an ORC system. In order to produce power from the multi-pressure flow streams, dual pressure cycle architectures proposed thus far have all required either multiple expanders or specially designed multi-stage expanders, capable of accepting the low pressure loop flow between the stages [7–11].

Single-stage turbine designs with multiple inlet chambers have a long history of use as “control stages” in steam turbine applications. In these designs, the turbine nozzles are grouped into a number of separate chambers which are placed around the rotor admission arc. Each chamber is connected to a separate control valve, which can be either fully opened or fully closed as needed to to adjust the total turbine mass flow and hence power produced. Since the source of steam is the same for all chambers, all active nozzle groups operate with the same supply pressure and temperature [12, 13].

Twin-entry radial-inflow turbines are also sometimes used in turbocharging applications in order to better balance the flow and pressure pulsations produced by the inherently unsteady engine exhaust [14, 15]. In these cases the inlet is divided into two 180 degree arc volute scrolls with each scroll feeding engine exhaust to half of the turbine rotor. The scrolls are connected to separate banks of engine cylinders in such a manner as to provide a more uniform supply of exhaust gas.

Neither of these applications allow for the efficient utilization of two separate flow streams, which are at fundamentally different pressure levels. To the best of the author’s knowledge, no single-stage turbine/expander technologies have been proposed that can produce power simultaneously from multiple flow streams at different pressure levels. This paper discusses the development and testing of such a turbine for use in a dual pressure ORC. This turbine concept is referred to as a dual-entry turbine (DET).

For the present work, using multiple expanders or a multi-stage expander to perform expansion from two different high side

pressures would be possible, however to enable more compact packaging, complexity reduction and cost savings, the use of a single-stage, DET expander is highly desirable. Increasing the cycle performance while minimizing cost helps achieve the necessary payback period desired by customers using class 8 trucks.

TEST PROGRAM

Cummins Inc. designed a full scale test loop for a dual pressure ORC system in order to demonstrate the achievable performance of the power cycle concept. Barber Nichols Inc. was contracted to design and manufacture the dual-entry turbine for the power cycle. The setup was first tested in a simulated engine test cell where the cycle parameters could be more carefully controlled and monitored. Following this test phase, the power cycle was installed and operated on an actual class 8 diesel engine to confirm the performance in the intended installed environment. Given the higher quality and quantity of data from the simulated engine test cell, all of the performance parameters presented herein come from the first phase of system testing, and only that test setup will be described.

Figure 1 shows the general layout of the dual pressure ORC and the heat sources. In addition to having two pressure levels, the high pressure loop of the cycle was also recuperated as shown. The working fluid of the power cycle was R1233zd(E) [16]. The system was configured to have separate feedpumps in parallel to supply the working fluid to the heat exchangers of the high and low pressure loops. The high pressure loop used a recuperator ahead of the high temperature heat exchanger to allow increased heat input to the high pressure loop flow and to increase the cycle efficiency and power production from the turbine expander. The recuperator was selected to be used on only the high pressure loop because the cycle efficiency of the high pressure loop is greater due to the increased pressure ratio across the turbine. The high pressure loop thus makes more efficient use of the heat added by the recuperator than the low pressure loop. Additionally, the gas side inlet temperatures and flows were sufficiently high that the recuperator matched well with the need for preheating liquid in the high pressure loop prior to accepting high temperature waste heat from the engine.

Both the high and low pressure loops were fed directly to the DET expander following heat addition into the ORC. The turbine expander has a common discharge for both fluid streams and this was input directly into the hot side of the recuperator. After de-superheating in the recuperator, the working fluid vapor was routed to the condenser to be condensed and subcooled prior to being supplied to the feedpumps to begin the cycle again.

During the thermodynamic cycle modeling, the temperatures of the waste heat sources were evaluated and similar temperature heat sources were grouped together to determine which sources would transfer heat to the low pressure and high pressure legs of the cycle. The lower temperature waste heat sources require a lower pressure because the saturation temperature of the working fluid needs to be kept below the temperature of the respective waste heat source in order for heat transfer to occur. Generally a high portion of the heat input is used for vaporization of the working fluid, therefore the saturation temperature creates a pinch point that must be examined. This thermal pinch often sets the maximum allowable pressure of the working fluid based on the available temperature of the heat source.

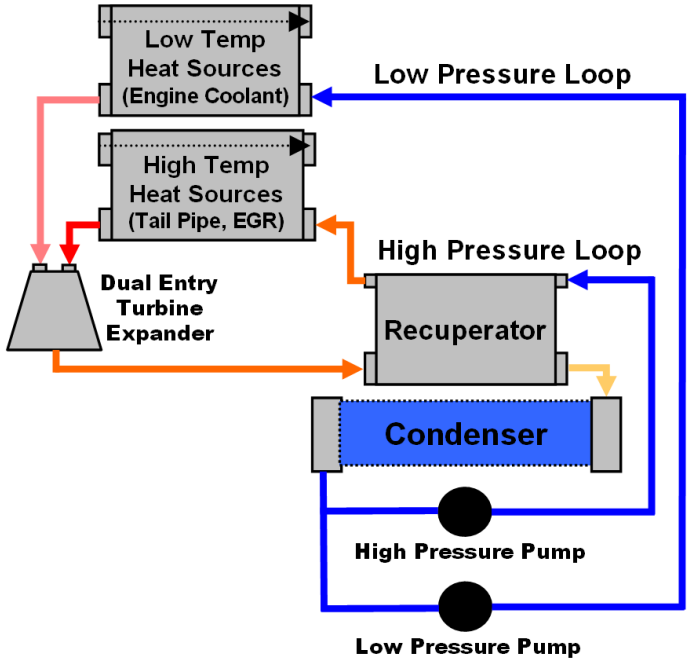

FIGURE 1. **Primary Components Of The Thermodynamic Cycle.**

The values of target superheat at the turbine inlet for both the high and low pressure streams were determined based on cycle optimization including evaluation of the thermal pinch points at the discharge of the heat exchangers. For the high pressure flow leg, higher superheat also allows for increased recuperated heat transfer, which in turn allows more flow to be made available to the inlet of the expander. The cycle was optimized for maximum net power from the system including several factors such as the amount of waste heat that can be extracted at a given high side pressure, the specific power of the working fluid and the effect of pump work. Higher pressures at the point of heat input result in a higher specific energy flow to the turbine, but there is a tradeoff between this and the corresponding required decrease in mass flow in order to produce a higher temperature flow for the given heat input. Further, increased high side pressure eventually reduces the quantity of waste heat that can be extracted due to thermal pinches. The effect of achievable turbine efficiencies at the varied conditions of the optimization must also be taken into

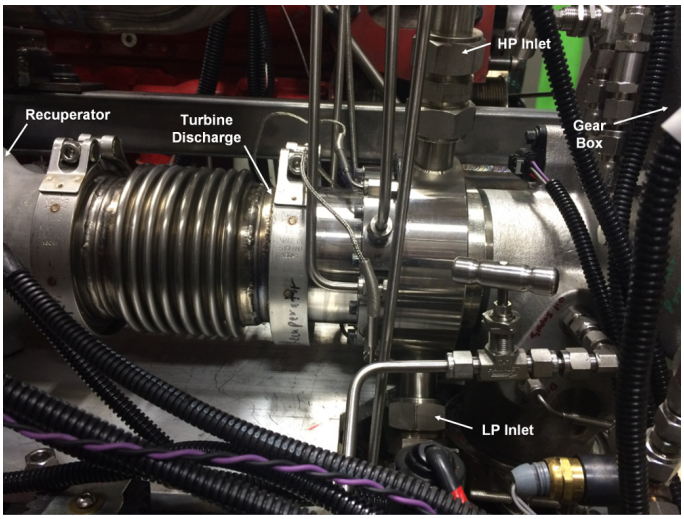

FIGURE 2. **The Dual-Entry Turbine Expander In The Installed Test Environment.**

consideration. The level of high side pressure and the amount of superheat for each leg of the cycle was determined by finding the maximum net turbine output power based on the evaluation of these trade factors.

The DET expander was operated in a test cell which is capable of simulating the heat rejection of a class 8 truck engine. The test cell utilizes two natural gas burners to provide heat input to the ORC in the form of exhaust gas directly and coolant heat rejection indirectly. The use of exhaust gas from the first burner simulates the high temperature heat sources from the engine. The coolant loop is heated using the second burner and is used to simulate the low temperature heat sources from the engine.

A class 8 truck diesel engine with the pistons and connecting rods removed was used as a fixture in the simulated engine test cell. The turbine expander was connected to a 10:1 ratio gearbox to reduce the turbine speed prior to transferring the turbine output power to the engine's crank pulley via a belt drive (see Figure 3). The supplementary power provided to the engine by the DET was measured by a torque sensor installed on the crank pulley in conjunction with a speed pickup, located on the output shaft of the gearbox. A dynamometer was installed on the opposite end of the engine crankshaft from the crank pulley and served as the primary load, and as a secondary power measurement for the DET.

DUAL-ENTRY TURBINE DESIGN CONSIDERATIONS

The nominal design parameters for the dual-entry turbine are provided in Table 1. The development of a DET that can extract power simultaneously from high and low pressure flow

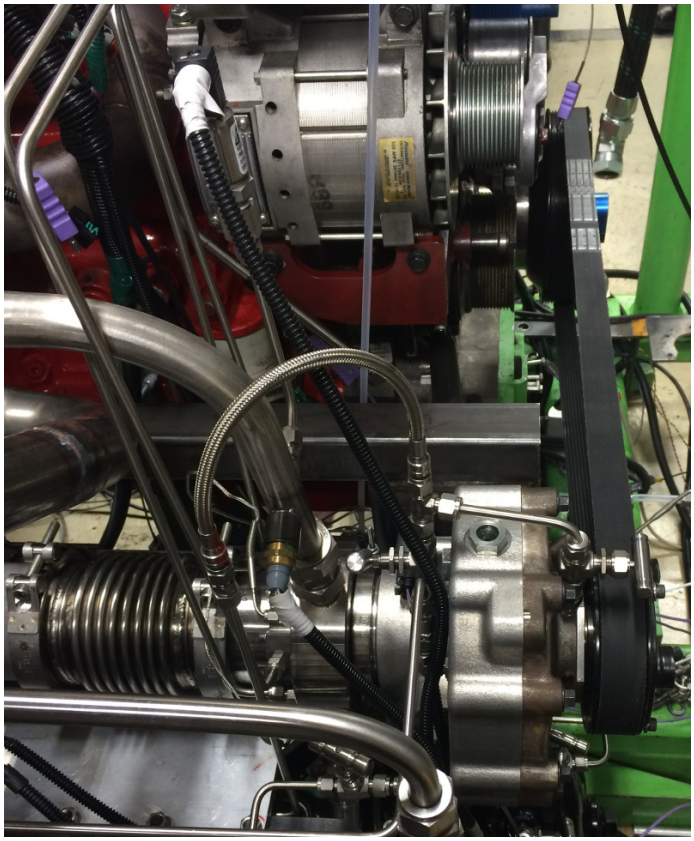

FIGURE 3. **The Turbine Speed Reduction Gearbox and Belt Drive Arrangement.**

streams is a challenging endeavor since the design parameters differ substantially between the two flow streams. In order to obtain optimal turbine performance, the nozzles and rotor blades must be designed in a complimentary manner so as to maintain proper turning of and alignment to the expanding flow. This is not possible to achieve for both flow streams with a single turbine. The overall design must therefore become a compromise between competing interests. Given the non-linear nature of many of the loss mechanisms that affect turbine performance, these compromises must be chosen carefully in order to obtain acceptable turbine performance.

A comparison of the values in Table 1 shows that the pressure ratio across the high pressure turbine nozzles is nearly three times that of the low pressure nozzles. This translates to approximately a 30% increase in the nozzle exit velocity for the high pressure flow relative to that of the low pressure flow. Additionally, the value of the specific speed, which is an indication of the appropriate shape factor for the turbine design [17–19], is 55% lower for the high pressure conditions than that of the low pressure conditions. The scale of these differences mean that if designed independently, the high and low pressure turbines would

TABLE 1. **Turbine Design Parameters For The Low and High Pressure Streams.**

Parameter	LP Turbine	HP Turbine
Turbine Type	Axial Impulse	Axial Impulse
Admission	62%	38%
P_{inlet} [*bara*]	11.44	31.0
T_{inlet} [$^{\circ}C$]	124.6	185.0
P_{exit} [*bara*]	2.17	2.17
PR_{ts} [ ]	5.25	14.3
Nozzle Mach # [ ]	1.80	2.25
C_o [m/s]	264.5	341.8
$\dot{m}$ [kg/s]	0.366	0.306
N [*RPM*]	28,000	28,000
U/C_o [ ]	0.446	0.345
N_s [ ]	0.217	0.140

have significantly different nozzle geometries, rotor diameters, wheel speeds, arcs of admission and blade heights.

The turbine inlet plenum was divided into two separate chambers, each with a unique bank of nozzles to handle the specific expansion requirements of the high and low pressure streams. In a large measure, the nozzles for the two streams were designed independently to accommodate the different pressure ratio and mass flow specifications. However, some compromise was made to the passage area distributions in order to decrease the disparity in a properly matched rotor blade height. The level of flow turning imparted by the nozzles was also adjusted away from optimum values in both nozzle banks in order to reduce the large variation in rotor blade incidence experienced as the blades pass from the arc of one flow stream to the other.

The blade height of the rotor was dictated by the mass flow continuity requirements of the low pressure stream, which had the highest volume flow. This means that the rotor blades are too tall for the high pressure stream, which leads to blade pumping losses in the dead portions of the blade that extend outside of the live nozzle jet.

The objective of the turbine is to extract as much energy as possible from the fluid streams. Any amount of remaining kinetic energy in the turbine discharge flow represents lost energy recovery. Of course some gas velocity is required to simply pass the flow through the turbine, and this component of velocity is governed by mass continuity relations. Efforts are therefore focused on reducing any tangential, or swirl velocity that remains in the exhaust stream of the turbine.

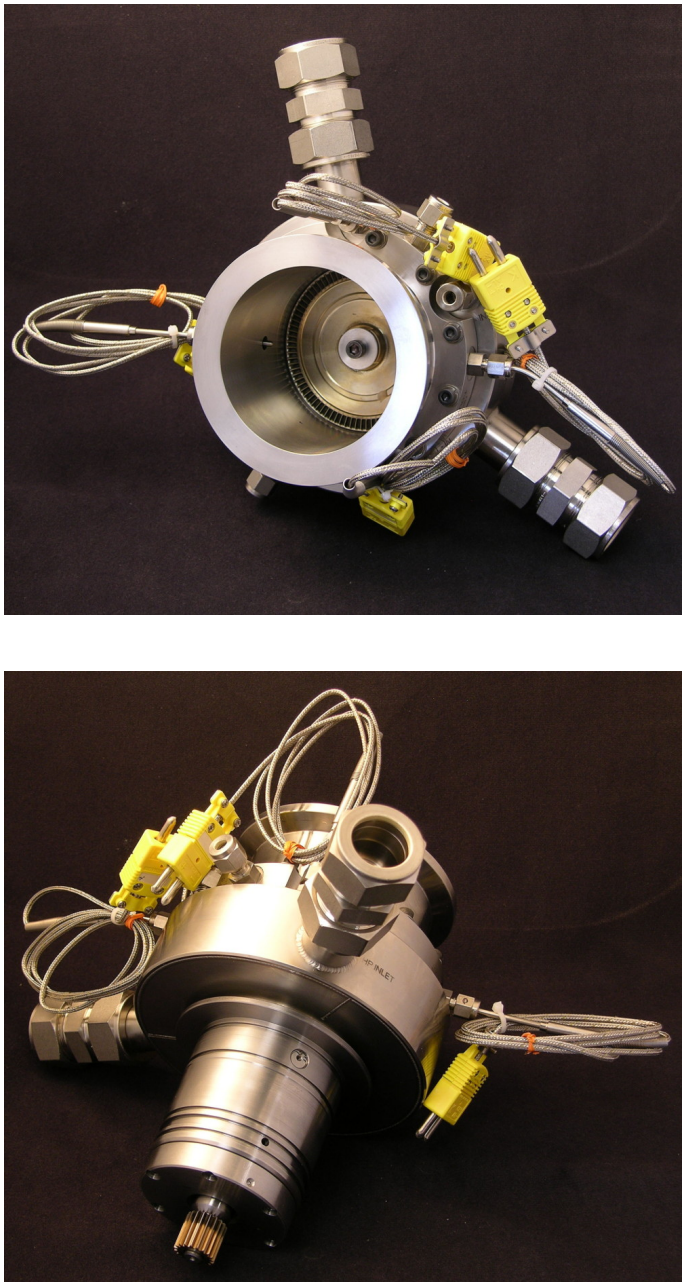

FIGURE 4. **Front And Aft Views Of The Dual-Entry Turbine Test Article.**

Generally, peak turbine hydraulic power will be realized when the exit swirl velocity component is eliminated all together. This is typically done by precise design of the blade profiles, and an appropriate selection of the blade speed. Given the large difference in gas velocities exiting the two nozzle banks, it is not possible to achieve this objective for both fluid streams. The composite design must therefore result from an effective man-

agement of the excess swirl between the two streams. The target blade speed identified by these trade offs is used in conjunction with the rotor diameter to determine the desired shaft speed of the turbine design.

The selection of the rotor diameter is another exercise of balancing conflicting requirements. As the rotor diameter is increased, a larger circumference is made available to the blades and nozzles. Mass continuity dictates that this must result in a reduction in the blade height, or the total arc of admission. Since each nozzle bank can only have an integer number of nozzles, and since each nozzle bank is required to pass its respective specified flow, the solution space becomes digital, possessing only discrete solutions of viable rotor diameters. Each solution corresponds to a specific blade height, nozzle count and arc of admission. An optimization was performed to minimize the combined losses that result from blade pumping on the high pressure arc, the dead space between nozzle banks (i.e. partial admission losses) and Reynold's number effects. The dual-entry turbine that resulted from this design process is shown in Figure 4.

PERFORMANCE PREDICTION METHODOLOGY

Performance predictions for the dual-entry turbine are not straight forward because the unique nature of the dual stream design falls outside of many empirical correlations that are typically used to estimate turbine performance. Further, the design also does not lend itself well to CFD based prediction methods due to the highly unsteady nature of the flow field as the rotor transitions from the flow exiting one nozzle bank to the other. Such a simulation would require a time-accurate solution and the likely requirement that a full 360 degree model be included into the computational domain. This type of analysis is very costly and would require substantial computational resources which were not supported by the program budget or schedule.

A method was therefore devised using turbine meanline prediction tools to provide a basis for estimating the net power and efficiency that can be expected from the DET concept. This method uses two different performance models to establish approximate upper and lower bound performance curves. The first model considers the DET to be represented by two separate, partial admission turbines; one representing the low pressure stream turbine, and the other representing that of the high pressure stream. Each of the turbines has identical nozzle and rotor geometry to the portion of the DET that they represent. The combined power output of these two turbine simulations is then taken to be representative of the net power produced by the DET. This method should provide conservative performance estimates since each of these turbines will incur full partial admission losses over the portion of arc that is, in actuality, occupied by the adjacent nozzle bank and flow stream. This model is thus used to provide the lower bound approximation (see Figures 7 & 8).

The second model considers the DET to be represented by two separate, full admission turbines. Similar to the first model, both turbines have identical nozzle and rotor geometry as their respective DET counterpart with the exception that for each, the mass flow is scaled up and nozzles are added until a full arc of admission is achieved. The net power produced is then scaled back down by the ratio of the original partial arc mass flow to the full arc mass flow. This process effectively removes any partial admission losses from the performance evaluation. This procedure is repeated for the other turbine representing the adjacent DET component.

In actuality, partial admission type losses do exist in the DET, even if there is no dead space between the adjacent nozzle banks. This is due to the blade scavenge losses that occur as the blades pass through the transition zone between the nozzle banks, as well as due to the blade pumping losses that occur in the high pressure arc resulting from the over sized rotor blade height. The second model is thus used to establish an upper bound for the turbine efficiency. The nominal prediction curve for the DET performance is taken as the arithmetic mean of the upper and lower curves (shown as dashed lines in Figures 7 & 8). Figure 5 shows the methodology that was used to construct the nominal prediction curve, where corresponding points on the upper and lower prediction curves were grouped and averaged.

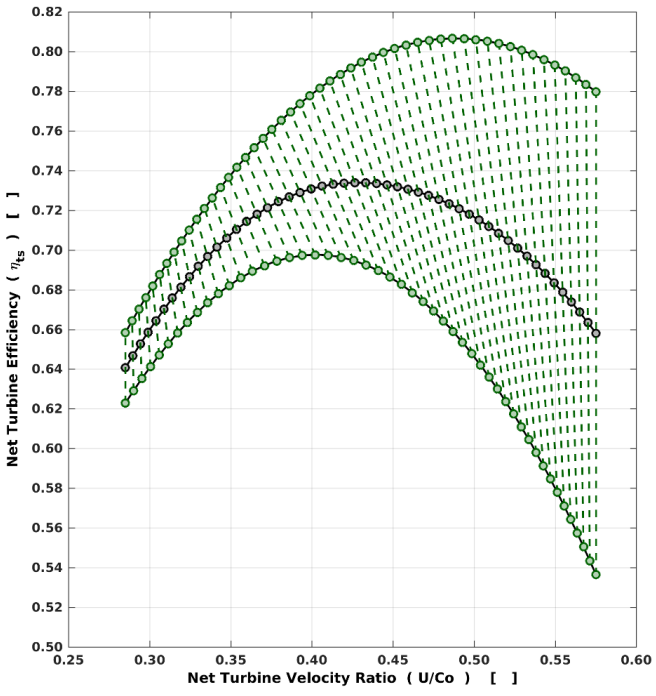

FIGURE 5. **Methodology Used To Establish The Nominal Prediction Curve.**

It is important to note that neither of these performance models account for any interaction effects between the two flow streams. Probably the most significant of these effects are the mixing losses that occur in the turbine exhaust duct behind the rotor. The large difference in velocity between the two flow streams can result in significantly different levels of swirl at the rotor discharge. As the two flow streams converge, mixing losses are incurred, and the energy associated with any dissipation of the tangential velocity component is converted into a combination of static pressure and temperature increases. A rise in the static pressure behind the rotor contributes directly to a reduction in the available energy that can be extracted by the turbomachinery.

Indirectly, a static temperature rise can also result in an increased turbine back pressure as the effect of a temperature increase is a lower gas density and hence higher volumetric flow rate, which drives an increase in duct pressure losses.

Other interaction effects not captured by this methodology include nozzle jet shear mixing losses driven by the velocity difference between adjacent nozzles of opposed flow streams, unsteady losses in the transition zones between nozzle banks, and heat transfer through the turbine housing from the high temperature to low temperature stream. The exclusion of these effects means that actual turbine performance is anticipated to favor the lower bound of the prediction curves.

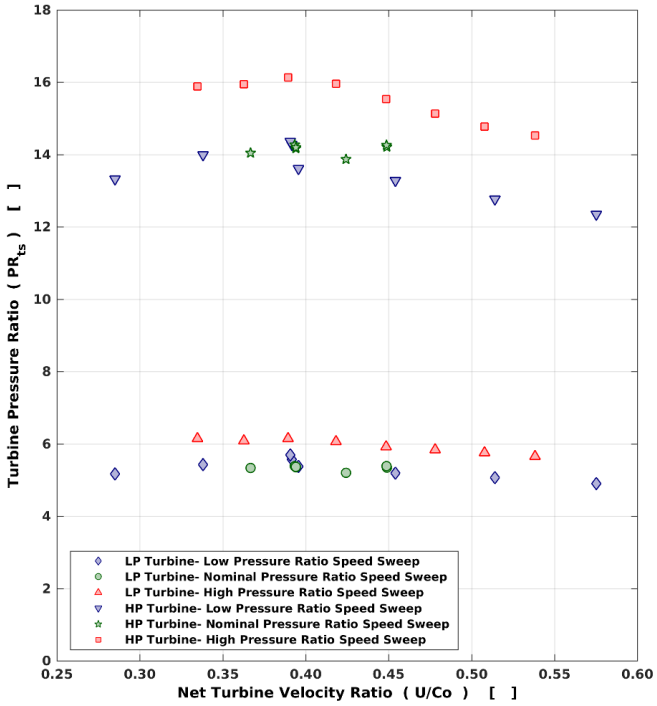

FIGURE 6. Pressure Ratio Variation From Intended Constant Pressure Ratio Operation. Error Bars Not Shown For Data Clarity.

TEST RESULTS

Throughout the ORC loop, pressures and temperatures were measured at the inlet and outlet of each component. For the dual-entry turbine specifically, pressure and temperature sensing ports were placed directly in the inlet plenums of each nozzle bank as well as in the discharge duct, clocked to circumferential locations that aligned with the discharge flow of the high and low pressure flow streams. The speed of the gearbox output shaft was measured using a speed probe. The turbine wheel speed was then obtained by multiplying this value by the 10:1 gearbox ratio.

Data obtained from operating the ORC test loop were reduced and processed in order to provide assessments of the DET performance. The NIST REFPROP [20] fluid property database was used to determine the thermodynamic state variables for the R1233zd(E) working fluid based on the pressure and temperature measurements.

As a general rule, turbine efficiency data plotted against the turbine velocity ratio, U/C_o, are expected to form a single characteristic curve shape. Excluding differences in Reynold's or Mach number effects, a given turbine geometry should achieve a consistent efficiency when operated at the same U/C_o condition regardless of the particular speed, temperature and pressures which correspond to the specific U/C_o value. For a supersonic turbine in particular, changes in the operating pressure ratio can produce Mach number effects (e.g. shock losses) which will cause deviations to this behavior, but such deviations are usually small unless the differences in pressure ratio are substantial.

Turbine performance trends are therefore usually most clear when the data are plotted against values of the turbine velocity ratio which are collected at fixed pressure ratios with varied shaft speed. To the extent possible, the data presented in the plots shown were obtained this way. However, control of the dual pressure loop ORC was complex and maintaining a fixed pressure ratio over time and a range of shaft speeds (power levels) required several dynamic variables to all be kept in balance. Figure 6 shows the level to which the high and low pressure ratios were able to be maintained at fixed values. All of the presented data correspond to these approximate constant pressure speed sweeps.

Since there was no practical way to independently measure the power produced separately by the high and low pressure flow streams of the DET, composite parameters had to be formulated in order to assess and characterize the turbine performance. The net efficiency of the DET is defined as:

$$\bar{\eta}_{ts} \equiv \frac{P}{(\dot{m}\Delta h_{s,ts})_{LP} + (\dot{m}\Delta h_{s,ts})_{HP}} \quad (1)$$

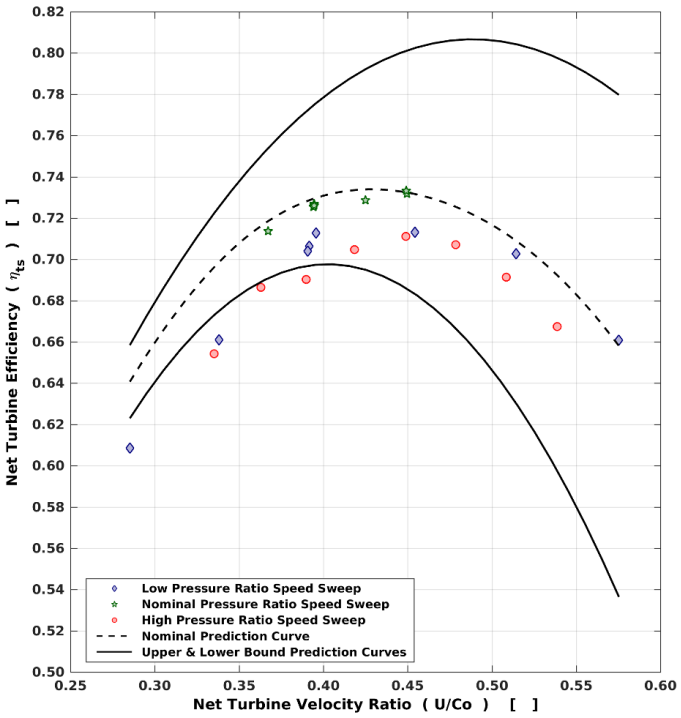

FIGURE 7. **DET Efficiency Data Derived From The Liquid Flow Rate Measurement.**

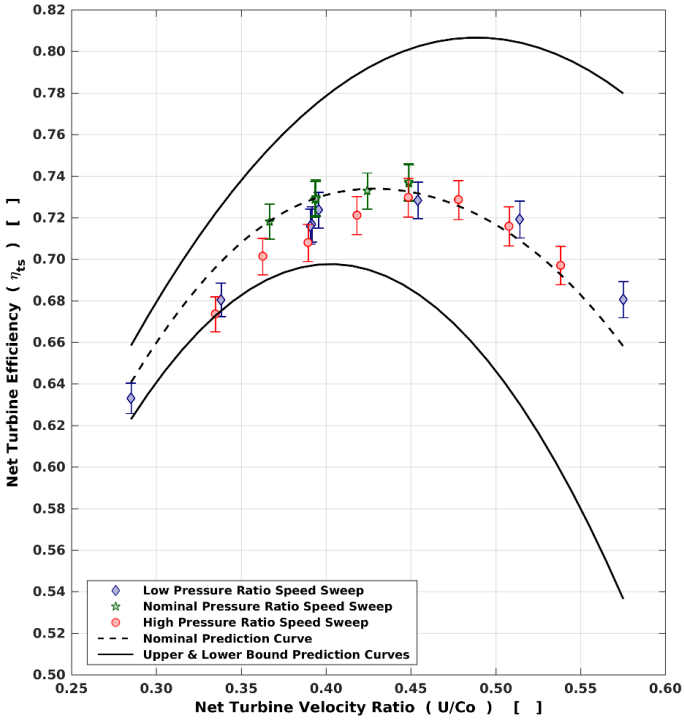

FIGURE 8. **DET Efficiency Data Derived From The Choked Nozzle Flow Rate Measurement.**

Similarly, the overall value of the spouting velocity is defined as:

$$\bar{C}_o \equiv \frac{(C_o \dot{m} \Delta h_{s,ts})_{LP} + (C_o \dot{m} \Delta h_{s,ts})_{HP}}{(\dot{m} \Delta h_{s,ts})_{LP} + (\dot{m} \Delta h_{s,ts})_{HP}} \tag{2}$$

The net value of U/C_o is then simply taken as the ratio of the blade wheel speed, which is the same for both fluid streams, and the calculated value of $\bar{C}_o$.

Two independent methods were employed to measure the flow rate of the working fluid in both legs of the power cycle. The liquid flow rate through each feedpump was measured using a volumetric flow meter. The mass flow was then determined by multiplying the resulting volume flows by the liquid density of the fluid.

A secondary flow measurement technique was used on the vapor side of the loop using the turbine nozzles themselves as flow meters. Since the pressure ratios across both nozzle banks are sufficient to produce supersonic flow, the nozzles can effectively function as choked-orifice flow meters [21]. The sizing of the nozzle throats are critical parameters to the turbine performance and are therefore carefully controlled features with tight tolerances. Following the manufacture of the nozzles, the throat area of each nozzle was measured and recorded. This data was used in conjunction with the plenum pressure and temperature measurements to calculate the choked mass flow rate through each nozzle bank.

The choked nozzle flow measurement method has been used successfully by the author many times in the past. For the present case the differences between the two measurement methods were a bit larger than expected. For the low pressure stream, the mass flow derived from the liquid side flow meter was an average of 2.2% higher than that of the choked flow value, with a standard deviation of 1.0%. Similar values of the mean and standard deviation for the high pressure stream were 0.74% and 1.5% respectively. The measured mass flow rate is a key parameter in the calculation of the turbine efficiency as indicated by Eqn. 1. The flow rate differences resulted in a discrepancy of upwards of two points in the calculated turbine efficiency. The efficiency data derived from the liquid flow rate measurements are shown in Figure 7, and the data reduced using the nozzle flow rates are presented in Figure 8.

In an effort to determine which of the flow measurements is most representative of the true mass flow rate, the data were

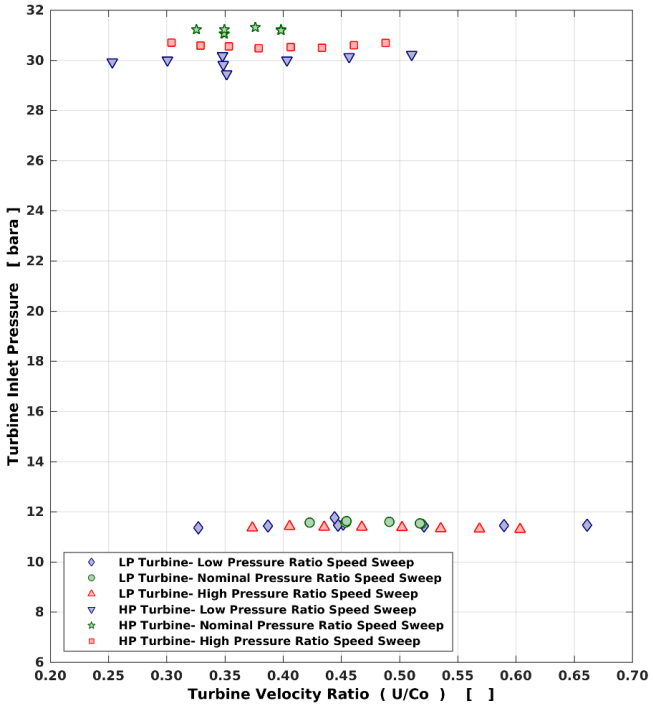

FIGURE 9. **Turbine Inlet Pressure. Error Bars Not Shown For Data Clarity.**

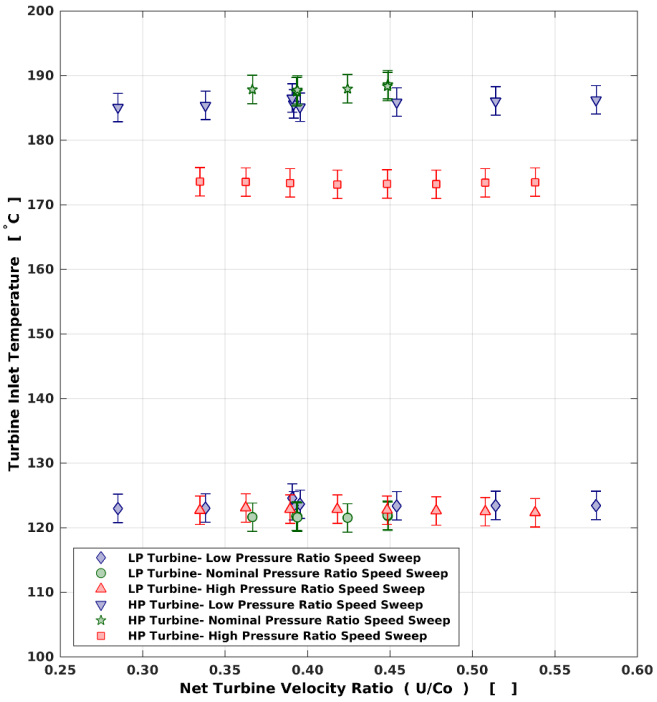

FIGURE 10. **Turbine Inlet Temperature Data.**

analyzed using the torque coefficient. The net torque coefficient is defined as:

$$\bar{\tau}_c \equiv \frac{\tau}{\dot{m}_{tot}\,\bar{C}_o\,D_{pitch}} \tag{3}$$

When the torque coefficient is plotted against the turbine velocity ratio, the extent to which the data conform to a linear relationship is an indication of the data quality [22].

Test data points that are not well stabilized, or are otherwise inconsistent will generally show up as outliers from the linear trendline. A torque coefficient plot of the data using the choked nozzle flow measurement is shown in Figure 12. The data plotted this way conform to a linear trend remarkably well, with an R-square value of 0.998. A similar analysis of the data based on the liquid flow rate measurements resulted in a 14.4% increase in the error. This would suggest that the choked nozzle flow measurement results are more physically valid. The data presented in Figure 8 are thus taken to be the data most representative of the turbine performance.

The argument to dismiss the liquid flow meter data is further supported by a closer examination of Figures 6 and 7. Despite the intent to operate the turbine at different pressure ratios between the nominal and low pressure ratio speed sweeps, the pressure ratios of the two data sets ended up largely overlapping (see Figure 6). Since the turbine is operating at the same non-dimensional state at these two conditions, there is no justifiable reason to explain the large efficiency discrepancy observed in Figure 7 between these data sets. The data of Figure 8 do a much better job of tending to form a common characteristic shape. This indicates that there may have been a calibration issue with the liquid flow meters.

Plots of the net power produced by the DET are given in Figure 11. Despite being at a similar pressure ratio and efficiency, the low pressure ratio data are lower than the nominal or high pressure ratio data due to a reduced turbine inlet pressure, and thus mass flow for this series relative to the others as indicated in Figure 9. Further, the reduced inlet pressure and temperature of the high pressure ratio data acted to largely offset the effect of a greater pressure ratio such that the net power of the high and nominal pressure ratio data converged to similar levels.

In order to provide a meaningful secondary measurement of the auxiliary power produced by the ORC, the dynamometer was operated in reverse as a motor with the DET drive belt removed to enable measurement of the parasitic power loss associated with rotating the crankshaft in the engine block (with pistons and connecting rods still removed). Parasitic loss data were collected over a range of speeds and at two different fixed engine oil temperature levels.

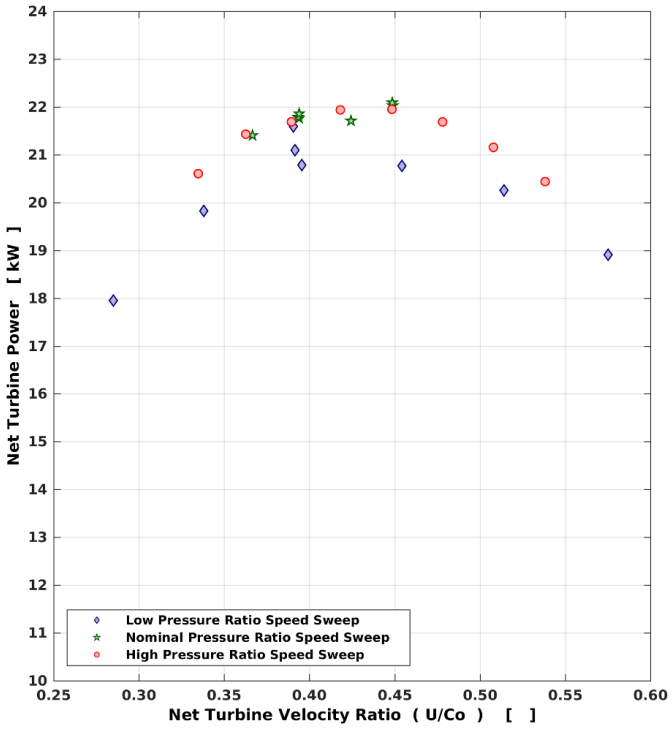

FIGURE 11. **Net Power Produced By The Dual-Entry Turbine At The Various Pressure Ratios. Error Bars Not Shown For Data Clarity.**

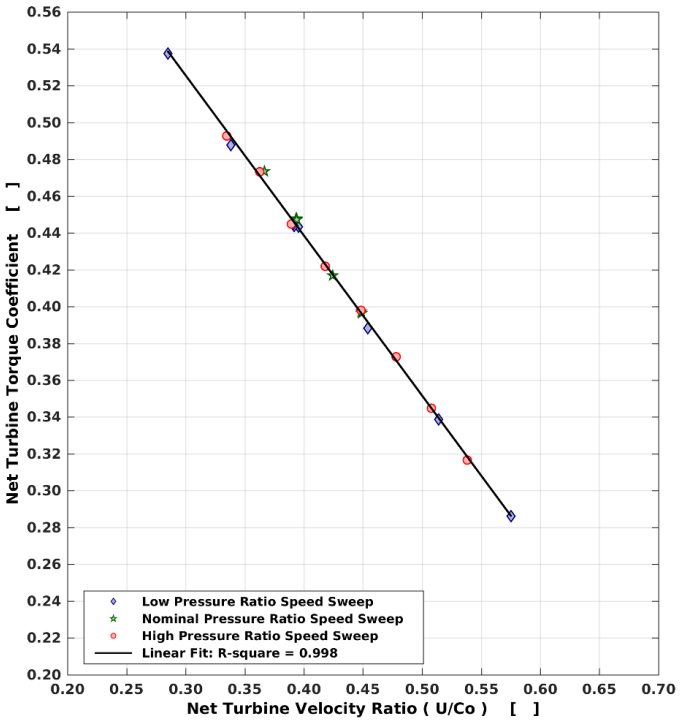

FIGURE 12. **Data Quality Assessment Using The Torque Coefficient Calculated From The Choked Nozzle Flow Measurements.**

When reducing the ORC test data, a bi-linear interpolation of the crankshaft parasitic data was made using the measured engine speed and oil pan temperature. The resulting calculated power loss was then added to the power measurement from the dynamometer in order to provide a comparison to the more direct, but sometimes less reliable, power measurement derived from the crank pulley torque meter.

During testing, the crank pulley torque meter signal would occasionally drop out due to poor electrical contact on the slip rings. Meaningful crank pulley torque meter data was present for the nominal and high pressure ratio data series, but was absent for the low pressure ratio data series (the lowest power data series). For the nominal and high pressure ratio data series, a direct comparison between the two power measurement methods was made, and the dynamometer based power measurement was determined to be an average of 0.97% lower than the power obtained from the crank pulley torque measurement, with a standard deviation of 0.26%. Due to the small number of data points that were used to determine the 0.97% offset, the low pressure ratio data series shown in Figure 11, was obtained directly from the dynamometer method without applying the 0.97% offset.

As seen in Figure 8, the nominal prediction curve seems to do a reasonable job of predicting the performance of the DET. At values of the turbine velocity ratio below about 0.45, the efficiency data fall off faster than predicted by the nominal curve, but are still above the lower bound curve. This is likely due to an interaction effect between the two flow streams that was not captured by the prediction methods. To investigate this further, the individual turbine meanline models used to produce the lower bound prediction curve were run at each of the test data points and evaluated for potential causes of the observed trends. It was observed from this analysis that at low values of U/C_o the tangential velocities exiting the rotor of both flow streams were highly negative, meaning that they were flowing in a direction opposite to the wheel rotation. At higher values of U/C_o, the tangential velocities of both streams switch direction and were of significant magnitude in the same direction as wheel rotation. The cross over points of these velocities for the low and high pressure streams were found to occur at a U/C_o values of approximately 0.40 and 0.47 respectively.

For partial admission turbines in particular, disk windage is a significant source of inefficiency. Since the lower bound, partial admission, turbine meanline models did not account for the disk windage effect of the negative or positive swirl velocities from the adjacent flow stream, it seems that this could be a reasonable cause for the observed trend.

UNCERTAINTY ANALYSIS

As previously noted, establishing a precise set of operating conditions with the dual pressure ORC proved to be rather difficult due to necessity to simultaneously keep a number of system parameters in balance. Further, the thermal conditioning of the piping and heat exchangers (i.e. operational history) had a significant influence on the ability to dial in a specific run point. For this reason, obtaining replicated data sets proved elusive, which eliminated the possibility of performing a statistical analysis on the data in order to determine confidence intervals for the total data uncertainty. The error bars shown in Figure 8 were thus derived from an analysis of the instrumentation measurement uncertainty only.

The turbine inlet pressure transducers for both the high and low pressure streams had a stated uncertainty of 0.08% of the full scale reading, which was 34.5 *bar*. This gives a measurement uncertainty of ± 0.03 *bar* for these sensors. The turbine discharge absolute pressure transducers had a range of 13.8 *bar*, thereby giving an uncertainty of ± 0.01 *bar*. The uncertainty associated with the pressure measurements was small enough to fall within the data markers in Figures 9 and 6 and were thus omitted from these plots for the sake of clarity.

The temperature probes for both the turbine inlet and discharge were required to be k-type thermocouples in order to be compatible with the already established data reduction system of the test cell. These sensors had a stated uncertainty of $\pm 2.2^{\circ}C$, which turned out to be the largest driver of the total uncertainty in the turbine efficiency measurement.

The throat area of the manufactured turbine nozzles were carefully measured with a total uncertainty of $\pm 0.14\%$ and 0.21% for the low and high pressure nozzle banks respectively.

Lastly, the measurement uncertainty of the crank pulley torque sensor was ± 0.2 *Nm*. The measurement uncertainty associated with the torque sensor was also small enough to fall within the data markers and were therefore also not shown in the power data of Figure 11. For the low pressure ratio data series, where the power was obtained from the dynamometer instead of the crank pulley torque sensor, it is recognized that there is an additional unknown uncertainty associated with the correlation of the crankshaft parasitic data to the speed and oil temperature data. Since these correlations were also not replicated, an independent assessment of the uncertainty associated with these correlations is not possible.

Due to limited remaining resources at the end of the test program, a statistical Monte Carlo type analysis of the effect of all the combined measurement uncertainties was not performed. Instead, the simpler approach of evaluating the turbine efficiency using the worst case stacking of all measurement uncertainties was used. The combinations of individual sensor uncertainties (plus or minus) which resulted in the largest reported turbine efficiency uncertainty were used to produce the error bars shown in Figure 8. Since, by the law of averages, random errors of a series of measurements with Gaussian distributions will tend to cancel out, the occurrence of such a worst case error stack is highly improbably and is thus a conservative estimate of the combined effect of the measurement errors on the turbine efficiency. The error bars shown in Figure 8 represent this conservative assessment of the combined measurement uncertainty.

CONCLUSIONS

Dual pressure ORC systems can help maximize power recovery from engine waste heat sources at varied temperature and quality. However, such dual pressure systems can be complex, costly and difficult to package. In order to offset many of these challenges, it is very desirable to expand both high and low pressure flow streams with a single turbine. For this purpose, a dual-entry turbine (DET) expander was developed, manufactured and tested. Data from the dual pressure ORC test loop have demonstrated the viability of the dual-entry turbine concept, and shown that the performance targets of the DET were achieved. The use of a dual pressure ORC with a DET expander can help large commercial vehicles, such as class 8 trucks, meet future goals of reducing emissions and increasing fuel economy.

ACKNOWLEDGMENT

The authors would like to thank the US DOE Office of Energy Efficiency & Renewable Energy for support of this work under contract award number DE-EE0007281.

REFERENCES

[1] Lecompte S., Huisseune H., van den Broek M., Vanslambrouck B., De Paepe M. *Review of Organic Rankine Cycle (ORC) Architectures for Waste Heat Recovery*, Renew. Sustain. Energy. Rev. 2015, 47:448-61.

[2] Shu G., Wang X., Tian H. *Theoretical Analysis and Comparison of Rankine Cycle and Different Organic Rankine Cycles as Waste Heat Recovery System For a Large Gaseous Fuel Internal Combustion Engine*, Appl. Therm. Eng. 2016, 108:525-37.

[3] Ma J., Liu L., Zhu T., Zhang T. *Cascade Utilization of Exhaust Gas and Jacket Water Waste Heat From an Internal Combustion Engine by a Single Loop Organic Rankine Cycle System*, Appl. Therm. Eng. 2016, 107:218-26.

[4] Shokati N., Ranjbar F., Yari M. *Exergoeconomic Analysis and Optimization of Basic, Dual-Pressure and Dual-Fluid ORCs and Kalina Geothermal Power Plants: A Comparative Study*, Renew. Energy 2015, 83:527-42.

[5] Li T., Zhang Z., Lu J., Yang J., Hu Y. *Two-stage Evaporation Strategy to Improve System Performance for Organic Rankine Cycle*, Appl. Energy 2015, 150:32334.

[6] Abadi G. B., Yun E., Kim K. C. *Experimental Study of a 1 kW Organic Rankine Cycle with a Zeotropic Mixture of R245fa/R134a*, Energy 2015, 93:236373.

[7] Manente G., Lazzaretto A., Bonamico E. *Design Guidelines for the Choice Between Single and Dual Pressure Layouts in Organic Rankine Cycle (ORC) Systems*, Energy 2017, 123:41331.

[8] Fontalvo A., Solano J., Pedraza C., Bula A., Quiroga A., Padilla R. *Energy, Exergy and Economic Evaluation Comparison of Small-Scale Single and Dual Pressure Organic Rankine Cycles Integrated with Low Grade Heat Sources*, Entropy Sep. 2017.

[9] Guzovic Z., Raskovic P., Blataric Z. *The Comparision of a Basic and a Dual-Pressure ORC (Organic Rankine Cycle): Geothermal Power Plant Velika Ciglena Case Study*, Energy 2014, 75:175-86.

[10] Smolen S. *Simulation and Thermodynamic Analysis of a Two-Stage Organic Rankine Cycle for Utilisation of Waste Heat at Medium and Low Temperature Levels*, Energy Sci. and Tech. 2011, 1:1:64-78.

[11] Peris B., Navarro-Esbri J., Moles F. *Bottoming Organic Rankine Cycle Configurations to Increase Internal Combustion Engines Power Output from Cooling Water Waste Heat Recovery*, Appl. Therm. Eng. 2013, 61:364-71.

[12] Church, E. F., 1935. *Steam Turbines*. McGraw-Hill, New York, NY.

[13] Singh, H. P. B. . M. P., 2009. *Steam Turbines: Design, Applications and Re-Rating*. McGraw-Hill, New York, NY.

[14] Romagnoli A., Copeland C.D., Martinez-Botas R., Seiler M., Rajoo S., Costall A. *Comparison Between the Steady Performance of Double-Entry and Twin-Entry Turbocharger Turbines*, J. Turbomach 2013, 135:011042.

[15] Cerdoun M., Ghenaiet A. *Characterization of a Twin-Entry Radial Turbine Under Pulsatile Flow Condition*, Int. J. Rot. Mach. 2016, 2016:4618298.

[16] Honeywell, 2017. Honeywell developed refrigerant known by trade name solstice. See also https://www.honeywell-refrigerants.com/americas/product/solstice-zd/.

[17] Balje, O. E., 1981. *Turbomachines*. John Wiley & Sons, New York, NY.

[18] Dixon, S. L., 1998. *Fluid Mechanics and Thermodynamics of Turbomachinery, 4th Edition*. Butterworth-Heinemann, Woburn, MA.

[19] Shepherd, D. G., 1956. *Principles of Turbomachinery*. Macmillan Publishing Company, New York, NY.

[20] Lemmon, E.W., Huber, M.L., McLinden, M.O. *NIST Standard Reference Database 23: Reference Fluid Thermodynamic and Transport Properties-REFPROP, Version 9.1*, May 2013. See also https://www.nist.gov/srd/refprop.

[21] Saad, M. A., 1993. *Compressible Fluid Flow, 2nd Edition*. Prentice-Hall Inc., Englewood Cliffs, NJ.

[22] Rolf H. Sabersky, Allan J. Acosta, E. G. H., 1989. *Fluid Flow - A First Course In Fluid Mechanics, 3rd Edition*. Macmillan Publishing Company, New York, NY.